Article

Not peer-reviewed version

Negative Mass in the Systems Driven by Entropic Forces

Edward Bormashenko *, Artem Gilevich, Shraga Shoval *

Posted Date: 30 July 2025

doi: 10.20944/preprints202505.1100.v3

Keywords: core-shell system; negative mass; negative density; entropic force; polymer spring; temperature dependence

 doi:10.20944/preprints202505.1100.v3

Article

Negative Mass in the Systems Driven by Entropic Forces

Edward Bormashenko [1,*], Artem Gilveich [1] and Shraga Shoval [2,*]

[1] Ariel University, Ariel, 407000, Israel, Engineering Faculty, Department of Chemical Engineering, Biotechnology and Materials

[2] Department of Industrial Engineering and Management, Faculty of Engineering, Ariel University, P.O. Box 3, Ariel 407000, Israel

* Correspondence: edward@ariel.ac.il

Abstract

The paper addresses the phenomena of the negative effective mass and negative effective density emerging in the systems driven by the entropic elastic forces. The elasticity of polymers is, at least partially, of entropic origin, and it represents the tendency of a polymer to evolve into a more probable state, rather than into one of lower potential energy. Entropy forces are temperature dependent; thus, the temperature dependence of the effective mass and effective density arises. The effect of the negative effective mass is a resonance effect, emerging in core-shell mechanical systems, which takes place when the frequency of the harmonic external force acting on core-shell system connected by an ideal spring, approaches from above to the eigen-frequency of the system. We address the situation when the ideal spring connecting core to shell is made from the polymer material, and its elasticity is of an entropic origin. The effective mass is calculated, and it is temperature-dependent. The chain of core-shell units connected with polymer spring is studied. The effective density of the spring is temperature dependent. Optical and acoustical branches of vibrations are elucidated. The negative mass and density become attainable under the variation of the temperature of the system. The situation, when only one of the springs demonstrates the temperature-dependent, entropic behavior is investigated. Exemplifications of the effect are addressed.

Keywords: core-shell system; negative mass; negative density; entropic force; polymer spring; temperature dependence

1. Introduction

Entropic forces are emergent forces that arise from the statistical tendency of a system to increase its entropy[1,2]. Unlike other fundamental forces (like gravity or electromagnetism), entropic forces originate from the system's tendency to maximize the number of accessible microstates [3]. Entropic origin of these forces represents the tendency of a system to evolve into a more probable state, rather than simply into one of lower potential energy [1]. Elasticity of polymers is driven to a much extent by entropy [4–7]. Maximizing entropy of a polymer chain implies reducing the distance between its two free ends. Consequently, an entropic elastic force emerges, that tends to collapse the chain. Elasticity of the muscles arises from entropy in a way very similar to the entropy-driven elasticity of polymer chains [8]. Entropic forces drive contraction of cytoskeletal networks [9]. Verlinde suggested that gravity is actually the entropic force [10]. According to Verlinde, gravity emerges from fundamental principles of statistical mechanics and information theory rather than being a fundamental interaction like electromagnetism. His idea is rooted in holographic principle and thermodynamics [10]. Verlinde showed that if information about matter is stored on a holographic screen (a surface encoding information about space), then the tendency of entropy to maximize leads

 doi:10.20944/preprints202505.1100.v3

to an effect that mimics Newton's law of gravity [10]. In a similar way the Coulomb interaction was treated as an entropic force [11].

Usually, entropic forces grow with temperature, however, the exceptions to this rule were reported, when the system of elementary magnets supposed to be in the thermal equilibrium with the thermal bath is exposed to external magnetic field [12]. A diversity of polymer materials demonstrate entropic elasticity, including rubber [13], Polydimethylsiloxane PDMS [14] and thermoplastic elastomers [15,16]. Entropic elasticity is inherent for tropocollagen, which is the building block of collagen fibrils and fibers that provide mechanical support in connective tissues [17]. Entropic elasticity was observed in slide-ring gels [18]. Somewhat surprisingly, entropic elasticity was reported in cubic crystals of ScF_3 [19].

Our paper addresses the situation when the entropic/polymer spring gives rise to the effect of the negative mass. The effect of the negative mass is a resonance effect, emerging in core-shell mechanical systems. This effect occurs when the frequency of the harmonic external force acting on core-shell system connected by a Hookean massless spring, approaches from above to the eigen-frequency of the system [20–24]. Negative-inertia converters for both translational and rotational motion were introduced [25].

The energy of the vibrated core-shell system is not conserved, due to the fact that it is exposed to the external harmonic force, as it occurs, for example, in the famous Kapitza pendulum, in which the pivot point vibrates in a vertical direction, up and down [26,27]. 2020). Unlike the Kapitza pendulum, the effect of "negative effective mass" arises in the linear approximation to the analysis of the motion [20–22,28]. The effect of the negative effective mass/negative effective density may be achieved with the plasma oscillations of the free electron gas in metals [29–31].

The effects of negative mass and negative density gave rise to the novel mechanic and thermal metamaterials [32–34]. The negative effective mass materials were manufactured by dispersion of soft silicon rubber coated heavy spheres in epoxy, acting as the mechanical resonators [20]. The negative density metamaterial was manufactured in an aluminum plate, comprising the resonant structure [35]. Soft 3D acoustic metamaterials polymer materials demonstrating negative effective density were reported [36]. Our paper is devoted to the possibility of realization of negative mass/density metamaterials exploiting entropic elastic forces.

2. Materials and Methods

Numerical calculations were performed with the Wolfram Mathematica software.

3. Results

3.1. Negative Mass in the Core-Shell System Driven by Entropic Elastic Force

Consider the core-shell mechanical system, depicted in Figure 1. The core mass m_2 is connected to the shell m_1 with two polymer stripes/springs. The entire system is subjected to the external sinusoidal force $Im(\hat{F}(t)) = F_{0x}sin\omega t$, as shown in Figure 1. We assume that the masses of the polymer stripes are much smaller than both masses of the core and shell; thus, the masses of polymer springs are negligible. The core-shell system may be replaced with a single effective mass m_{eff} expressed with Eq. 1 (for the rigorous derivation of Eq. 1, see: [23,24,28,29].

$$m_{eff} = m_1 + \frac{m_2\omega_0^2}{\omega_0^2-\omega^2}, \quad (1)$$

where $\omega_0 = \sqrt{\frac{2k}{m_2}}$, and k is the elastic constant of the polymer stripe (the core mass is driven by the pair of polymer springs).

 doi:10.20944/preprints202505.1100.v3

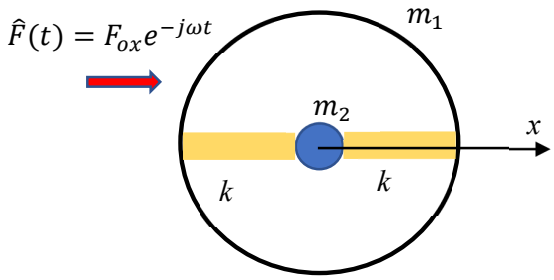

Figure 1. The core-shell unit giving rise to the effect of the "negative effective mass". The core mass m is connected with two polymer elastic Hookean springs k to the shell m_1. The core-shell system is exposed to the harmonic external force $\hat{F}(t) = F_{ox}e^{-j\omega t}$.

It is easily seen from Eq. 1 that, when the frequency ω approaches ω_0 from above, the effective mass m_{eff} will be negative [21,22,28,29] . For the sake of simplicity we assume that the polymer stripe/spring is built of ξ identical polymer chains, each of which may be represented by the ideal Kuhn equivalent freely jointed chain, built of N Kuhn monomers, the length of the Kuhn segment is b [5]. The elastic constant k of the polymer spring is given by Eq. 2:

$$k = 3\xi\frac{k_BT}{Nb^2}, \tag{2}$$

where k_B is the Boltzmann constant, and T is the temperature; we assume that the temperature is constant along the addressed core-shell system [5]. Substitution of Eq. 2 into Eq. 1 yields for the effective mass of the entire core-shell system (the masses of the polymer springs are neglected):

$$m_{eff}(\omega,T) = m_1 + \frac{\frac{6\xi k_BT}{Nb^2}}{\frac{6\xi\,k_BT}{m_2Nb^2} - \omega^2} \tag{3}$$

Now we fix the frequency of the external force ω, and vary the temperature of the core-shell system T. It is easily seen, that the effective mass $m_{eff}(\omega,T)$ becomes negative when the temperature of the core-shell system approaches the critical temperature T^* from below, where T^* is given by Eq. 4:

$$T^* = \frac{m_2N(b\omega)^2}{6\xi k_B} \tag{4}$$

The dependence $m_{eff}(T)$ is presented in Figure 2 (the value of ω is fixed). It is instructive to calculate the asymptotic values of $m_{eff}(T)$. When, $T \gg T^*$we derive from Eq 3.

$$\lim_{T\gg T^*} m_{eff}(T) = m_1 + m_2 \tag{6}$$

which is intuitively clear for an infinitively stiff spring. The low-temperature limit of the effective mass is also easily calculated.

$$\lim_{T\ll T^*} m_{eff}(T) = m_1 \tag{7}$$

Eq. 7 is also intuitively clear; indeed, the influence of the "weak" polymer spring (the temperatures are low) becomes negligible.

 doi:10.20944/preprints202505.1100.v3

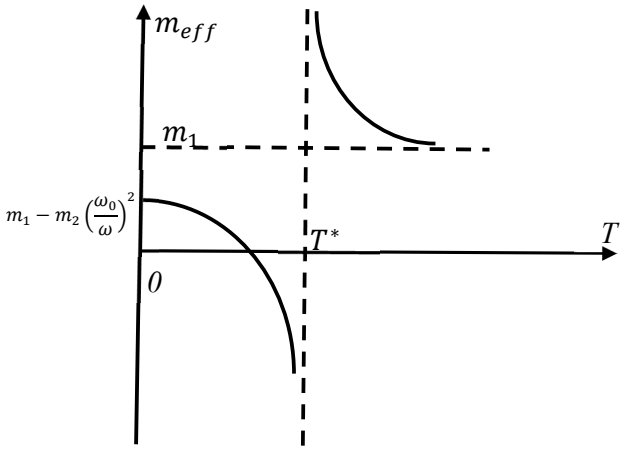

Figure 2. Temperature dependence of the effective mass $m_{eff}(T)$ is depicted. $T^* = \frac{m_2 N (b\omega)^2}{6\xi k_B}$. Dashed lines demonstrate the asymptotic behavior of $m_{eff}(T)$.

3.2. Negative Density of the Chain of Core-Shell Systems Driven by Elastic Forces

The concept of negative resonant density emerging in the chain of core-shell units, depicted in Figure 3, was introduced [29]. The effective density of the chain depicted in Figure 3; $\rho_{eff}(\omega)$, was calculated in [29]; and it is given by Eq. 8:

$$\rho_{eff}(\omega) = \rho_{st} \frac{\theta}{\delta(1+\theta)\left(\frac{\omega}{\omega_0}\right)^2} \left\{ cos^{-1}\left\{ 1 - \frac{\delta}{2\theta} \frac{\left(\frac{\omega}{\omega_0}\right)^2 \left[\left(\frac{\omega}{\omega_0}\right)^2 - (1+\theta)\right]}{\left(\frac{\omega}{\omega_0}\right)^2 - 1} \right\} \right\}^2 \tag{8}$$

where m_1 and m_2 are the masses of the shell and core correspondingly, the linear density of the chain ρ_{st} is given by: $\rho_{st} = \frac{m_1+m_2}{a}$; $[\rho_{st}] = \frac{kg}{m}$ and $\theta = \frac{m_2}{m_1}$; $\delta = \frac{k_2}{k_1}$; and a is the lattice constant (see Figure 3), $\omega_0 = \sqrt{\frac{k_2}{m_2}}$. It was demonstrated that the effective density becomes negative, when the frequency of external force ω approaches ω_0 from above [29].

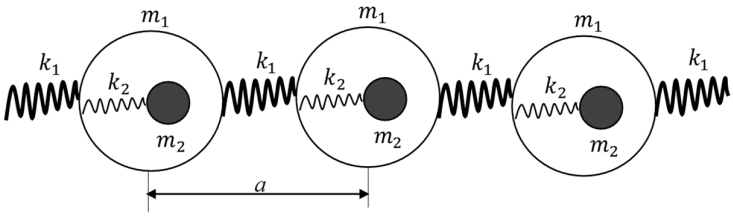

Figure 3. Chain of the core-shell units giving rise to the effect of temperature dependent negative density [22]. The single lattice constant of the 1D chain, defined as the distance between the core-shell units is a, the mass of the core is m_1, the mass of the shell is m_2, k_1 and k_2 are entropic strings.

Now we assume that both of the springs are polymer stripes. The elasticity of the stripes is given by Eqs. 9-10 [5]:

$$k_1 = 3\xi_1 \frac{k_B T}{N_1 b_1^2} = \alpha_1 T, \tag{9}$$

 doi:10.20944/preprints202505.1100.v3

$$k_2 = 3\xi_2 \frac{k_B T}{N_2 b_2^2} = \alpha_2 T, \tag{10}$$

where $\xi_i, N_i, b_i, i = 1,2$ are the numbers and parameters of the Kuhn chains, constituting the strings, $\alpha_i = 3\xi_i \frac{k_B}{N_i b_i^2}, i = 1,2$. It is noteworthy that the parameter; $\delta = \frac{k_2}{k_1}$ is temperature-independent. Thus, the squared resonant frequency ω_0^2 is given by Eq. 11:

$$\omega_0^2 = 3\xi_2 \frac{k_B T}{m_2 N_2 b_2^2} = \frac{\alpha_2 T}{m_2} \tag{11}$$

where $\alpha_2 = 3\xi_2 \frac{k_B}{N_2 b_2^2}$. Hence, the effective density of the chain appears as follows:

$$\rho_{eff}(\omega, T) = \rho_{st} \frac{\theta}{\delta(1+\theta)\frac{m_2\omega^2}{\alpha_2 T}} \left\{ cos^{-1}\left\{ 1 - \frac{\delta}{2\theta} \frac{\frac{m_2\omega^2}{\alpha_2 T}\left[\frac{m_2\omega^2}{\alpha_2 T} - (1+\theta)\right]}{\frac{m_2\omega^2}{\alpha_2 T} - 1} \right\} \right\}^2 \tag{12}$$

Now we fix the frequency of the external force ω. The plot $\rho_{eff}(T)$ is depicted in **Figure 4**. The graph is numerically built with Wolfram Mathematica software. The blue curve depicts the dependence $\rho_{eff}(\omega, T)$ for the dimensionless parameters: $k_1 = k_2 = 1 \times T$; $m_1 = 1$; $\delta = 1$; $\theta = m_2$; $a = 1$; $\omega = 2.3$; $m_2 = 20$.

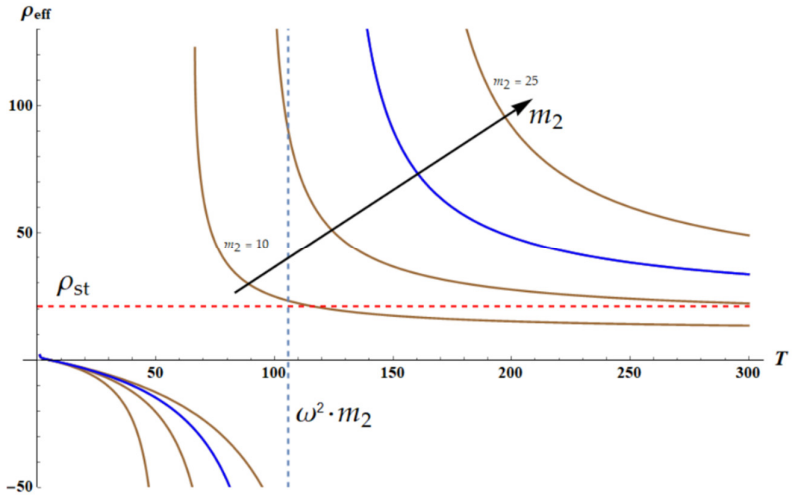

Figure 4. The temperature dependent effective density of the chain, shown in Figure 3 is depicted. The blue curve depicts the dependence $\rho_{eff}(\omega, T)$ for the dimensionless parameters: $k_1 = k_2 = 1 \times T$; $m_1 = 1$; $\delta = 1$; $\theta = m_2$; $a = 1$; $\omega = 2.3$; $m_2 = 20$ The resonance occurs when $T^* = \omega^2 m_2$. Set of brown curves depicts the temperature dependencies of the effective density calculated for the different values of $10 \le m_2 \le 25$ Blue dashed line demonstrates the asymptotic behavior of $\rho_{eff}(T)$. Red dashed line is $\rho_{eff} = \rho_{st} = \frac{m_1+m_2}{a}$. Black arrow depicts increase in m_2.

It is recognized that $\rho_{eff}(T)$ becomes negative, when the temperature of the core-shell system approaches to the critical temperature T^* from below, where T^* is given by Eq. 13:

$$T^* = \frac{\omega^2 m_2}{\alpha_2}, \tag{13}$$

where $\alpha_2 = 3\xi_2 \frac{k_B}{N_2 b_2^2}$. Set of the brown curves, appearing in **Figure 4**, depicts the temperature dependencies of the effective density $\rho_{eff}(T)$ calculated for the different values of $10 \le m_2 \le 25$. It is easily demonstrated that the high-temperature limit of the effective density is given by Eq. 14:

$$\lim_{T\to\infty} \rho_{eff}(\omega, T) = \rho_{st} = \frac{m_1+m_2}{a}, \tag{14}$$

which is well-expected for the massless, infinitely stiff springs.

Let's vary the parameter δ in Eq. 8 in the range less and greater than one, namely $0.7 < \delta < 1.3$. Parameter $\delta = \frac{k_2}{k_1}$ quantifies relative stiffness of spring k_2 referred to the string k_1. The variation of parameters m_2 and δ is illustrated with **Figure 5**. Brown curves are built for the fixed $\delta = 1$ and

 doi:10.20944/preprints202505.1100.v3

demonstrate change of ρ_{eff} with ω for $10 \le m_2 \le 25$. Magenta curves, in turn, illustrate are built for fixed $m_2 = 20$ and $0.7 < \delta < 1.3$.

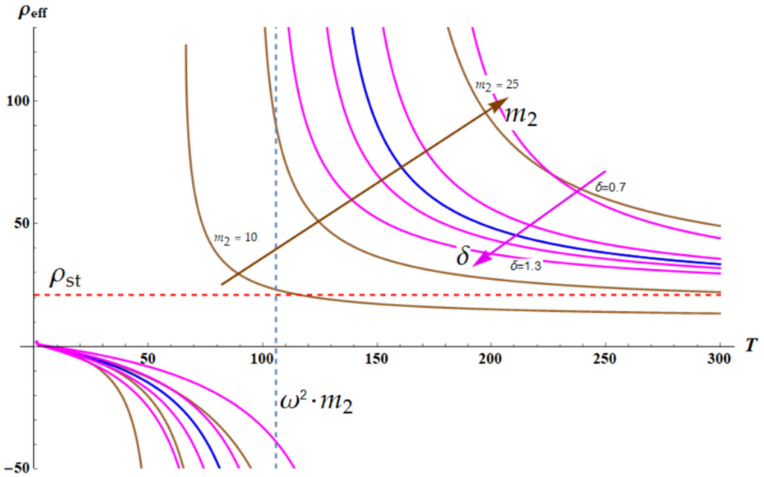

Figure 5. The plots demonstrate change in the resonance curves when parameters m_2 and δ are varied. Brown curves are built for the fixed $\delta = 1$ and demonstrate change of ρ_{eff} with ω for $10 \le m_2 \le 25$. The blue curve demonstrates $\rho_{eff}(T; \omega = 2.3, m_2 = 20, \delta = 1)$. The magenta curves illustrate variation in $0.7 < \delta < 1.3$ and depict $\rho_{eff}(T; \omega = 2.3, m_2 = 20, \delta \in \{0.7, 0.9, 1.1, 1.3\})$. Brown arrow depicts increase in m_2; magenta arrow illustrates increase in δ.

Figure 5 illustrates the very important result, increase in $\delta = \frac{k_2}{k_1}$ leads to the sharpening of the resonance behavior of $\rho_{eff}(T)$ dependence. This result is intuitively quite understandable; indeed, the decrease in stiffness of the outer spring k_1 results in the sharpening of the resonance.

The dependence $\rho_{eff}(\delta)$ as calculated for different temperatures is depicted in **Figure 6**. In the low temperature limit, when $T \ll \omega^2 m_2$ and, $\delta \ll 1$ the effective density $\rho_{eff}(T, \omega)$ almost doesn't change with $\delta = \frac{k_2}{k_1}$, as it is illustrated with **Figure 6**.

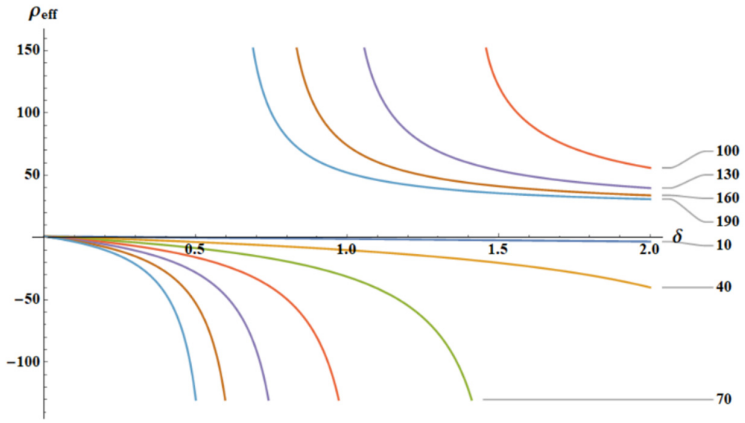

Figure 6. The dependence $\rho_{eff}(\delta)$ is depicted for various temperatures T. The curves $\rho_{eff}(\delta; \omega = 2.3, m_2 = 20, T \in [10, 190])$ are depicted.

Now we address a situation, when we remove the temperature dependence of the elasticity of the stripes (Eqs 9-10) one by one. The first case: $k_1(T) = T$, $k_2 = const(T) = 1$. Then Eq. 8 with dimensionless parameters will transform to Eq. 15:

 doi:10.20944/preprints202505.1100.v3

$$\rho_{eff}(T;\omega,\alpha_2) = \frac{T}{\omega^2} cos^{-1}[1 - \frac{\omega^2(-1-m_2+\omega^2 m_2)}{2T(-1+\omega^2 m_2)}]^2 \quad (15)$$

The dependence $\rho_{eff}(T)$ calculated for the different values of parameter m_2 is illustrated with **Figure 7**.

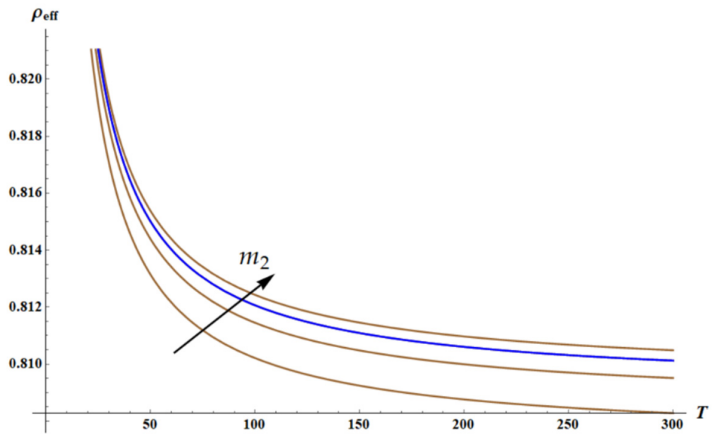

Figure 7. Curves $\rho_{eff}(T;\ m_2 \in \{10, 15, 20\ (Blue), 25\}, \omega = 2.3)$ are depicted. Black arow depicts the increase in m_2. $\lim_{T\to\infty}\left(\rho_{eff}(T,\omega)\right) = 1 + \frac{m_2}{1-\omega^2 m_2}$.

The second case corresponds to $k_1 = const(T) = 1,\ k_2(T) = T$. Then Eq. 8 with dimensionless parameters will transform to Eq. 16:

$$\rho_{eff}(T,\omega) = \frac{1}{\omega^2} cos^{-1}[1 - \frac{\omega^2(-1-m_2+\frac{\omega^2 m_2}{T})}{2(-1+\frac{\omega^2 m_2}{T})}]^2 \quad (16)$$

The dependence $\rho_{eff}(T)$ calculated for the different values of parameter m_2 is illustrated with **Figure 8**.

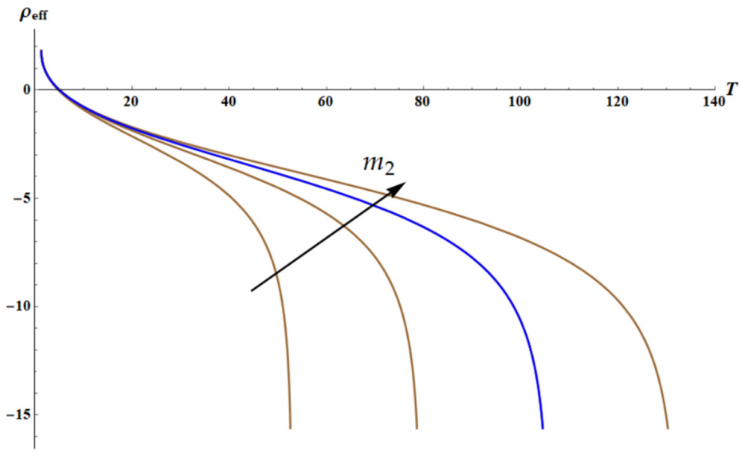

Figure 8. Here are curves $\rho_{eff}(T;\ m_2 \in \{10, 15, 20\ (Blue), 25\}, \omega = 2.3)$. The asymptotic behavior corresponds to $T = \omega^2 m_2$. Black arrow depicts the increase in m_2.

The field of negative densities is clearly recognized in **Figure 8**.

3.3. Dispersion Equations: Influence of the Temperature

 doi:10.20944/preprints202505.1100.v3

The dispersion equation for the 1D lattice (**Figure 3**) is given by [29–31]:

$$m_1 m_2 \omega^4 - [(m_1 + m_2)k_2 + 2k_1 m_2(1 - \cos(qa))]\omega^2 + 2k_1 k_2(1 - \cos(qa)) = 0. \quad (17)$$

Considering, as earlier, the dimensionless parameters: $m_1 = 1$; $\delta = 1$; $\theta = m_2$; $a = 1$ Eq. 17 yields:

$$m_2 * \omega^4 - \big((1 + m_2)k_2(T) + 2m_2 * k_1(T)(1 - \cos(q)\big)\omega^2 + 2k_1(T) * k_2(T)(1 - \cos(q) = 0. \quad (18)$$

For $k_1(T) = T$, $k_2(T) = T$ (both of springs are entropic) we have:

$$\frac{1}{(T/m_2)^2} * \omega^4 - \big((1 + m_2) + 2m_2 * (1 - \cos(q)\big)\frac{\omega^2}{T/m_2} + m_2 2(1 - \cos(q) = 0. \quad (19)$$

It is clear that the solution of the dispersion equation (**Figure 9**) does not depend on temperature for $\frac{\omega(q)}{\omega_0} = \frac{\omega(q)}{\sqrt{\frac{k_2}{m_2}}} = \frac{\omega(q)}{\sqrt{\frac{T}{m_2}}}$.

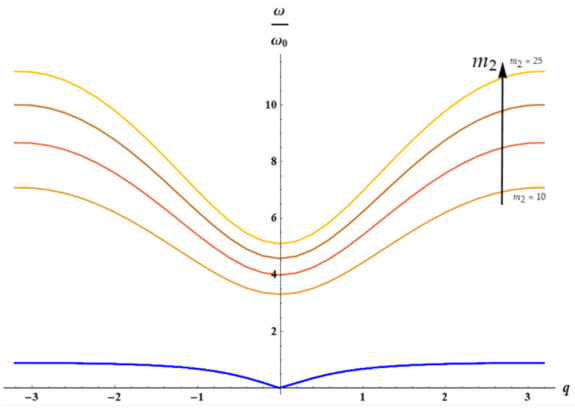

Figure 9. The solution of dispersion equation (Eq. 19) is depicted: acoustic (blue curves) and optical branches (from brown ($m_2 = 10$) to orange ($m_2 = 25$) curve), calculated for $m_2 \in \{10, 15, 20, 25\}$. The arrow indicates the direction of increase in parameter m_2 value. It is seen that dependence of acoustic mode on m_2 for $m_2 \gg 1$: $m_2 \in \{10, 15, 20, 25\}$ is negligible.

Let's consider two cases $k_1 = 1, k_2 = T$ (only spring k_2 is entropic) and $k_1 = T, k_2 = 1$ (only spring k_1 is entropic).

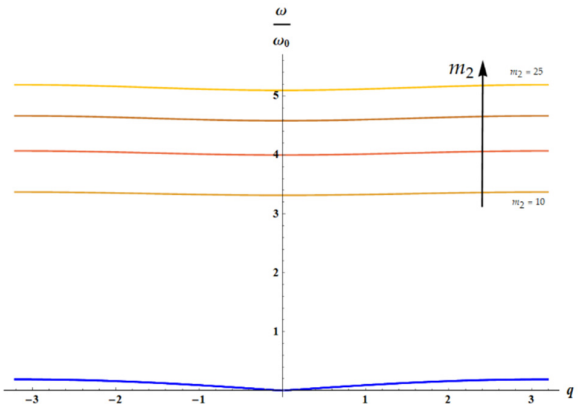

Figure 10. The solution of dispersion equation (Eq. 18) for $k_1 = 1, k_2 = T$ is depicted: acoustic (blue curves) and optical branches (from brown ($m_2 = 10$) to orange ($m_2 = 25$) curve), calculated for $m_2 \in \{10, 15, 20, 25\}$. The arrow indicates the direction of increase in parameter m_2 value.

 doi:10.20944/preprints202505.1100.v3

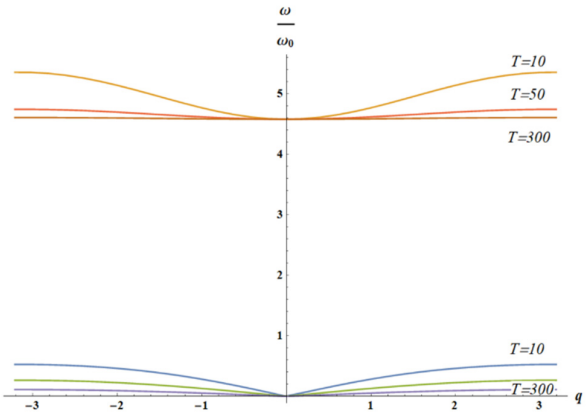

Figure 11. The solution of dispersion equation (Eq. 18) for $k_1 = 1, k_2 = T$ is depicted. Here $m_2 = 20$; $T \in \{10, 50, 300\}$. It is evident that with increasing temperature T both acoustic (blue, green and purple) and optical branches (orange, red, brown) depend weakly on the wave vector q.

Figure 12 and **Figure 13** illustrate the situation, when optical branch of the vibrations is strongly temperature-dependent; whereas, acoustic branch is slightly temperature dependent.

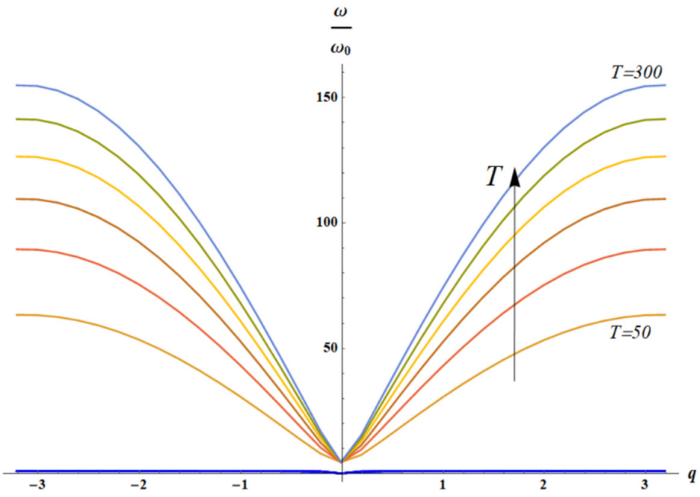

Figure 12. The solution of dispersion equation (Eq. 18) for $k_1 = T, k_2 = 1$ is depicted acoustic (blue curves) and optical branches (from brown ($m_2 = 10$) to orange ($m_2 = 25$) curve), calculated for $m_2 \in \{10, 15, 20, 25\}$. The arrow indicates the direction of increase in parameter m_2 value.

 doi:10.20944/preprints202505.1100.v3

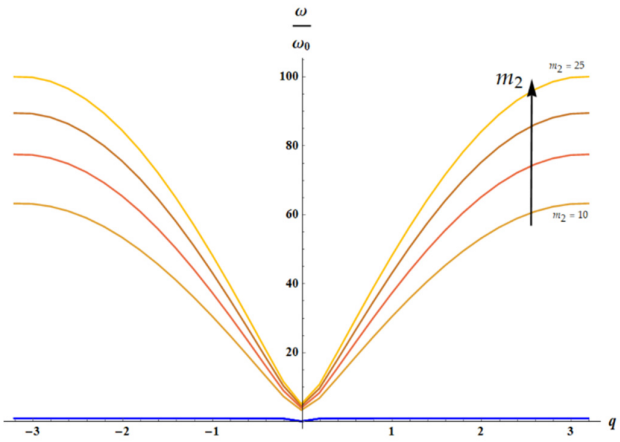

Figure 13. The solution of dispersion equation (Eq. 18) for $k_1 = T, k_2 = 1$ is depicted. Here $m_2 = 20$; temperature T changes from 50 (orange "optical" branch) to 300 (light blue "optical" curve) with a step of 50. Acoustic branch (blue curves) is barely dependent on temperature.

4. Discussion

Resonances are ubiquitous in nature and engineering [37–39]. It is well known, that the resonant phenomena may be temperature dependent. The temperature dependence of the resonance frequency of the fundamental and four higher order modes of a silicon dioxide micro-cantilever was established [40]. Temperature effects in resonant Raman spectroscopy were registered [41]. Temperature dependent Raman resonant response in UO_2 was reported [42]. The temperature dependence of the Fano resonance discovered in infrared spectra of nano-diamonds was discussed [43]. We address the temperature dependent resonant effects giving rise the phenomenon of the "negative effective mass effect", exerted to the intensive research in the last decade.

It is unnecessary to say that actually there is no negative mass [29,44,45]. The phenomenon of the "negative effective mass" arises when we substitute the core-shell mechanical systems comprising a pair of masses (M and m) and the massless Hookean spring k by a single effective mass m_{eff}, that is to say that the internal mass m is hidden and its influence is expressed by the introduction of the mass m_{eff} [21–23,29,44]. The negative effective mass represents the contra-intuitive situation of "anti-vibrations", when the harmonic acceleration of the system is in an opposite direction to the sinusoidal applied force [21–23,28,29]. We considered the situation when the vibrations are driven by temperature-dependent entropic forces, inherent for natural and biological polymer systems [13–19,46]. The stiffness of the polymer spring is temperature-dependent, and the physical situation resembling the parametric resonance emerges, when the temperature is varied [45]. Thus, the temperature-dependent effective mass emerges. The effect may be exemplified with polymer acoustic meta-materials [36,47]. The temperature dependent effective mass is not a novel concept; it is broadly used in semiconductors [48]. However, in our analysis the effect of temperature dependent mass emerges from the entropic origin of the elastic force in resonant systems.

The engineering realization of suggested approach may be realized with rubbers or thermoplastic elastomers [14–16]. Negative density materials exploiting thermoplastic materials were already reported [49]. In particular, negative mass system/waveguide based on styrene butadiene rubber were introduced [50]. These systems have a potential for the temperature-dependent negative mass behavior.

5. Conclusions

We conclude that the effect of the temperature-dependent effective mass becomes possible in the core-shell systems in which the spring connecting the core mass to the shell is driven by the temperature-dependent entropic elasticity, such as that inherent for polymer materials. The core-shell

 doi:10.20944/preprints202505.1100.v3

system may be replaced with a single effective mass $m_{eff}(\omega, T)$ exposed to the external harmonic force. When the frequency of the external force ω is fixed and the temperature of the core-shell system T is varied, the resonance becomes possible, and the harmonic acceleration of the shell may move in an opposite direction to the applied force. We demonstrate that the effective mass $m_{eff}(T)$ becomes negative when the temperature of the core-shell system approaches to the critical temperature T^* from below.

We also considered the chain/lattice built of core-shell units, in which entropic forces are acting. In this case, the effect of "negative density" is attainable under variation the temperature of the system. Again, the negative density $\rho_{eff}(T, \omega)$ becomes negative when the temperature of the core-shell system approaches the critical temperature T^* from below. The critical temperature is defined by the parameters of polymer chain and frequency of the external force ω. We varied the parameters of the lattice built of the core-shell elements and connected with the elastic springs. Increase in the stiffness of the springs connecting the core-shell units, leads to the sharpening of the resonance behavior of $\rho_{eff}(T)$ dependence. We also addressed a situation, and calculated the resonance curves, when we removed the temperature dependence of the elasticity of the "inner" and "outer" elastic elements one by one. In the low temperature limit, the effective density $\rho_{eff}(T, \omega)$ almost doesn't change with the ratio of the elastic constants of the "internal" and "external springs" appearing in the lattice. . Optical and acoustical branches of vibrations are calculated. The effect may be demonstrated experimentally with polymer meta-materials.

Author Contributions: Edward Bormashenko: Conceptualization, methodology, validation, formal analysis, investigation, writing—original draft preparation. Artem Gilevich: Formal analysis, investigation, writing—original draft preparation. Shraga Shoval: Conceptualization, methodology, validation, investigation, writing—original draft preparation.

Funding: This research received no external funding.

Institutional Review Board Statement: Not applicable.

Informed Consent Statement: Not applicable.

Data Availability Statement: The original contributions presented in this study are included in the article. Further inquiries can be directed to the corresponding author.

Acknowledgments: The authors are thankful to anonymous reviewers for extremely fruitful reviewing of the manuscript.

References

1. Taylor, P.L.; Tabachnik, J. Entropic Forces—Making the Connection between Mechanics and Thermodynamics in an Exactly Soluble Model. *Eur J Phys* **2013**, *34*, 729–736, doi:10.1088/0143-0807/34/3/729.
2. Wissner-Gross, A.D.; Freer, C.E. Causal Entropic Forces. *Phys Rev Lett* **2013**, *110*, 168702, doi:10.1103/PhysRevLett.110.168702.
3. Sokolov, I.M. Statistical Mechanics of Entropic Forces: Disassembling a Toy. *Eur J Phys* **2010**, *31*, 1353–1367, doi:10.1088/0143-0807/31/6/005.
4. Gedde, U.W. *Polymer Physics*; Springer Netherlands: Dordrecht, 2001; ISBN 978-0-412-62640-1.
5. Rubinstein, M.; Colby, R.H. *Polymer Physics*; 1st ed.; Oxford University Press, 2003; ISBN 019852059X.
6. Graessley, W.W. *Polymeric Liquids & Networks*; Garland Science, 2003; ISBN 9780203506127.
7. Kartsovnik, V.I.; Volchenkov, D. Elastic Entropic Forces in Polymer Deformation. *Entropy* **2022**, *24*, 1260, doi:10.3390/e24091260.
8. Tskhovrebova, L.; Trinick, J.; Sleep, J.A.; Simmons, R.M. Elasticity and Unfolding of Single Molecules of the Giant Muscle Protein Titin. *Nature* **1997**, *387*, 308–312, doi:10.1038/387308a0.
9. Braun, M.; Lansky, Z.; Hilitski, F.; Dogic, Z.; Diez, S. Entropic Forces Drive Contraction of Cytoskeletal Networks. *BioEssays* **2016**, *38*, 474–481, doi:10.1002/bies.201500183.

 doi:10.20944/preprints202505.1100.v3

10. Verlinde, E. On the Origin of Gravity and the Laws of Newton. *Journal of High Energy Physics* **2011**, *2011*, 29, doi:10.1007/JHEP04(2011)029.
11. Wang, T. Coulomb Force as an Entropic Force. *Physical Review D* **2010**, *81*, 104045, doi:10.1103/PhysRevD.81.104045.
12. Bormashenko, E. Magnetic Entropic Forces Emerging in the System of Elementary Magnets Exposed to the Magnetic Field. *Entropy* **2022**, *24*, 299, doi:10.3390/e24020299.
13. Treloar, L. R. G. *The Physics of Rubber Elasticity*, 3rd ed.; Clarendon Press: Oxford, 1975.
14. Paul, J. Thermoelastic characterization of carbon nanotube reinforced PDMS elastomer, *J. Polym. Eng*. **2021**, 41 (2), 87-9415.
15. Park, H.; Park, S.; Park, J. M.; Sung, B. J. Entropic contribution to the nonlinear mechanical properties of thermoplastic elastomers, *Macromolecules* **2025**, *58* (4), 1993–2004.
16. Arruda, E.M.; Boyce, M.C. A three-dimensional constitutive model for the large stretch behavior of rubber elastic materials, *J. Mech. Phys. Solids*, 1**993**, *41*, 389–412.
17. Buehler, M. J.; Wong, S. Y. Entropic elasticity controls nanomechanics of single tropocollagen molecules, *Biophysical J*. **2007**, *93* (1), 37-43.
18. Ito, K. Novel entropic elasticity of polymeric materials: why is slide-ring gel so soft? *Polym. J*. **2012**, *44*, 38–41.
19. Wendt, D.; Bozin, E.; Neuefeind, J.; Page, K.; Ku, W.; Wang, L.; Fultz, B.; Tkachenko, A. V. Zaliznyak, I.A. Entropic elasticity and negative thermal expansion in a simple cubic crystal, *Science Adv*. **2019**; *5*, eaay2748.
20. Liu, Z.; Zhang, X.; Mao, Y.; Zhu, Y.Y.; Yang, Z.; Chan, C.T.; Sheng, P. Locally Resonant Sonic Materials. *Science (1979)* **2000**, *289*, 1734–1736, doi:10.1126/science.289.5485.1734.
21. Chan, C.T.; Li, J.; Fung, K.H. On Extending the Concept of Double Negativity to Acoustic Waves. *Journal of Zhejiang University-SCIENCE A* **2006**, *7*, 24–28, doi:10.1631/jzus.2006.A0024.
22. Milton, G.W.; Willis, J.R. On Modifications of Newton's Second Law and Linear Continuum Elastodynamics. *Proceedings of the Royal Society A: Mathematical, Physical and Engineering Sciences* **2007**, *463*, 855–880, doi:10.1098/rspa.2006.1795.
23. Liu, X.N.; Hu, G.K.; Huang, G.L.; Sun, C.T. An Elastic Metamaterial with Simultaneously Negative Mass Density and Bulk Modulus. *Appl Phys Lett* **2011**, *98*, doi:10.1063/1.3597651.
24. Yang, M.; Ma, G.; Yang, Z.; Sheng, P. Coupled Membranes with Doubly Negative Mass Density and Bulk Modulus. *Phys. Rev. Lett.* **2013**, *110*, 134301, doi:10.1103/PhysRevLett.110.134301.
25. Lončar, J.; Igrec, B.; Babić, D. Negative-Inertia Converters: Devices Manifesting Negative Mass and Negative Moment of Inertia. *Symmetry* **2022**, *14*, 529, doi:10.3390/sym14030529.
26. Ramachandran, R.; Nosonovsky, M. Vibro-Levitation and Inverted Pendulum: Parametric Resonance in Vibrating Droplets and Soft Materials. *Soft Matter* **2014**, *10*, 4633–4639, doi:10.1039/C4SM00265B.
27. Hasan, M.S.; Nosonovsky, M. Method of Separation of Vibrational Motions for Applications Involving Wetting, Superhydrophobicity, and Microparticle Extraction. *Phys Rev Fluids* **2020**, *5*, 054201, doi:10.1103/PhysRevFluids.5.054201.
28. Bormashenko, E. *Bioinspired Materials and Metamaterials*; CRC Press: Boca Raton, 2025; ISBN 9781003178477.
29. Huang, H.H.; Sun, C.T.; Huang, G.L. On the Negative Effective Mass Density in Acoustic Metamaterials. *Int J Eng Sci* **2009**, *47*, 610–617, doi:10.1016/j.ijengsci.2008.12.007.
30. Bormashenko, E.; Legchenkova, I. Negative Effective Mass in Plasmonic Systems. *Materials* **2020**, *13*, 1890, doi:10.3390/ma13081890.
31. Bormashenko, E.; Legchenkova, I.; Frenkel, M. Negative Effective Mass in Plasmonic Systems II: Elucidating the Optical and Acoustical Branches of Vibrations and the Possibility of Anti-Resonance Propagation. *Materials* **2020**, *13*, 3512, doi:10.3390/ma13163512.
32. Kshetrimayum, R.S. A Brief Intro to Metamaterials. *IEEE Potentials* **2005**, *23*, 44–46, doi:10.1109/MP.2005.1368916.
33. Karami, B.; Ghayesh, M.H. Dynamics of Graphene Origami-Enabled Auxetic Metamaterial Beams via Various Shear Deformation Theories. *Int J Eng Sci* **2024**, *203*, 104123, doi:10.1016/j.ijengsci.2024.104123.

 doi:10.20944/preprints202505.1100.v3

34. Wang, Y.; Qin, Y.; Luo, K.; Tian, Q.; Hu, H. Dynamic Modeling and Simulation of Hard-Magnetic Soft Beams Interacting with Environment via High-Order Finite Elements of ANCF. *Int J Eng Sci* **2024**, *202*, 104102, doi:10.1016/j.ijengsci.2024.104102.
35. Sang, S.; Mhannawee, A.; Wang, Z. A Design of Active Elastic Metamaterials with Negative Mass Density and Tunable Bulk Modulus. *Acta Mech* **2019**, *230*, 1003–1008, doi:10.1007/s00707-018-2320-2.
36. Brunet, T.; Merlin, A.; Mascaro, B.; Zimny, K.; Leng, J.; Poncelet, O.; Aristégui, C.; Mondain-Monval, O. Soft 3D Acoustic Metamaterial with Negative Index. *Nat Mater* **2015**, *14*, 384–388, doi:10.1038/nmat4164.
37. Feynman, R. *The Feynman Lectures on Physics*; Addison Wesley Publishinng Co. Reading: Massachusetts, **1964**.
38. Ogata, K. *System Dynamics*; 4th ed.; Pearson, **2003**.
39. Manevitch, L.I.; Gendelman, O. V. *Tractable Models of Solid Mechanics*; Foundations of Engineering Mechanics; 1st ed.; Springer Berlin Heidelberg: Berlin, Heidelberg, **2011**; ISBN 978-3-642-15371-6.
40. Sandberg, R.; Svendsen, W.; Mølhave, K.; Boisen, A. Temperature and Pressure Dependence of Resonance in Multi-Layer Microcantilevers. *Journal of Micromechanics and Microengineering* **2005**, *15*, 1454–1458, doi:10.1088/0960-1317/15/8/011.
41. Fantini, C.; Jorio, A.; Souza, M.; Strano, M.S.; Dresselhaus, M.S.; Pimenta, M.A. Optical Transition Energies for Carbon Nanotubes from Resonant Raman Spectroscopy: Environment and Temperature Effects. *Phys Rev Lett* **2004**, *93*, 147406, doi:10.1103/PhysRevLett.93.147406.
42. Livneh, T. Resonant Raman Scattering in UO2 Revisited. *Phys Rev B* **2022**, *105*, 045115, doi:10.1103/PhysRevB.105.045115.
43. Shiryaev, A.A.; Ekimov, E.A.; Prokof'ev, V.Y. Temperature Dependence of the Fano Resonance in Nanodiamonds Synthesized at High Static Pressures. *Jetp. Lett*. **2022**, *115*, 651–656.
44. Yao, S.; Zhou, X.; Hu, G. Experimental Study on Negative Effective Mass in a 1D Mass–Spring System. *New J Phys* **2008**, *10*, 043020, doi:10.1088/1367-2630/10/4/043020.
45. Landau, L.; Lifshitz, E. *Mechanics: Volume 1 (Course of Theoretical Physics S)*; Butterworth-Heinemann, **2000**.
46. Rico-Pasto, M.; Ritort, F. Temperature-dependent elastic properties of DNA, *Biophysical Reports*, **2022**, *2* (3), 100067.
47. Fok, L.; Zhang, X. Negative Acoustic Index Metamaterial. *Phys Rev B* **2011**, *83*, 214304, doi:10.1103/PhysRevB.83.214304.
48. Cavassilas, N.; Autran, J.-L.; Aniel, F.; Fishman, G. Energy and temperature dependence of electron effective masses in silicon, *J. Appl. Phys*. **2002**, *92*, 1431–1433.
49. Lai, Y.; Wu, Y.,;Sheng, P.; Zhang, Z-Q. Hybrid elastic solids. *Nature Mater*. **2011**, *10*, 620–624. https://doi.org/10.1038/nmat3043
50. Yao, Sh.; Zhou, X.; Hu, G. Investigation of the negative-mass behaviors occurring below a cut-off frequency, *New J. Phys*. **2010**, *12*, 103025. DOI 10.1088/1367-2630/12/10/103025